# Phonon mechanism for the orthorhombic distortion in $FeSi_2$ as compared to cubic $CoSi_2$

S. Sanguinetti, C. Calegari,* V. R. Velasco,† G. Benedek, F. Tavazza, and Leo Miglio
*Istituto Nazionale per la Fisica della Materia and Dipartimento di Fisica dell'Università di Milano, Via Celoria 16, 20133 Milano, Italy*
(Received 6 May 1996)

We analyze the leading role of the electron-phonon interaction in promoting the structural distortion from fluorite to orthorhombic $FeSi_2$ by comparing a tight-binding calculation of the force constants and phonon dispersion relations in $FeSi_2$ to the ones in $CoSi_2$, a related compound which is stable in fluorite phase. [S0163-1829(96)07037-3]

## I. INTRODUCTION

Metallic $CoSi_2$ and $NiSi_2$ are stable in the fluorite structure and, due to the good matching to the silicon lattice, they have been considered for epitaxial deposition of very sharp Schottky junctions.[1] On the contrary, a related compound such as $FeSi_2$ is not bulk stable in the $CaF_2$ ($\gamma$) phase, which however displays a metallic density of states very similar to $CoSi_2$.[2] Actually, the room-temperature stable phase, $\beta$-$FeSi_2$, is a moderate distortion of the $CaF_2$ structure, which has 48 atoms in the one-face-centered orthorhombic cell.[3] Still, recent experiments by molecular beam epitaxy have demonstrated that fluorite $\gamma$-$FeSi_2$ can be stabilized at very low coverage on Si(111) (Ref. 4) due to a lower interface energy with respect to the orthorhombic phase.[5] By increasing the film thickness a structural transition to the $\beta$ phase takes place, which is supposed to be driven by the high electronic density of states (DOS) at the Fermi level in $\gamma$-$FeSi_2$.[6]

An important indication of the Fermi level position being critically important for the distortion comes from a very recent molecular dynamics simulation at variable cell shape for both $\gamma$-$FeSi_2$ and $CoSi_2$,[7] showing that the former naturally transforms into the semiconducting $\beta$ phase, whereas the latter, which has the Fermi level in a region of lower density, is substantially stable in the fluorite structure. If the actual mechanism acting in the pretransformation stage is the sizeable coupling between the electronic bands and the lattice distortion, a large electron-phonon coupling should be present and its effects should result in the appearance of phonon instabilities.

In order to check this point we have performed the calculation of the phonon dispersion relations both in $CoSi_2$ and $FeSi_2$ fluorite phases. We adopt a semiempirical approach for the estimation of the real-space force constants, where the repulsive part of the interatomic potential is a phenomenological function to be fitted to available elastic and optical data, whereas the attractive (covalent) part is given by a summation over the occupied one-electron states. To this end the tight-binding method is particularly well suited, since it provides the electronic contributions to the force constant matrix in a simple, still reliable way. Details about this method are given in Sec. II, where the evaluation of the long range and short range effects is performed separately by means of a Green function perturbative scheme in the atomic displacements.

Actually the inclusion of all the long-range interactions produced by the electronic polarization is important even for (stable) $CoSi_2$, since large flat portions of the Fermi surface generate a high susceptibility at $2k_F$ ($k_F$ is the Fermi wave vector). This is a major effect in fluorite $FeSi_2$ and in Sec. IV we discuss the convergence of elastic and vibrational parameters within the parameterization outlined in Sec. III. In Sec. V we report our results for the phonon bands which display imaginary frequencies only in the case of $FeSi_2$ indicating the sensitivity of the lower optical branches to the position of the Fermi level. Here we show that $LO_1$ bears the most important part of the electron-phonon interaction both in $CoSi_2$ and $FeSi_2$. In our opinion, it is the phonon instability mostly responsible for the structural distortion in $\gamma$-$FeSi_2$, since it provides a displacement pattern in agreement with the target phase.

## II. CALCULATION PROCEDURE

In this work we adopt the orthogonal tight-binding (TB) scheme for the calculation of the total energy $E_{\rm tot}$ of the crystal as a function of the atomic position $\{\mathbf{R}\}$. It has been very successful in the estimation of phonon dispersion relations for silicon,[8] graphite,[9] and transition metals.[10] The potential energy of the system, which includes the electronic kinetic energy and the core-electron, core-core, and electron-electron terms, can be rewritten as the sum of one band structure contribution plus one empirical repulsive term

$$E\{\mathbf{R}\}=E_{\rm kin}+E_{c\text{-}e}+E_{c\text{-}c}+E_{e\text{-}e}=E_{\rm bs}\{\mathbf{R}\}+E_{\rm rep}\{\mathbf{R}\}. \quad (1)$$

The former is given by a sum over the one-electron occupied states

$$E_{\rm bs}=\sum_{n,\mathbf{k}} \epsilon_{n,\mathbf{k}} f(\epsilon_{n,\mathbf{k}}-E_F), \quad (2)$$

where $n$ indicates the band index, $\mathbf{k}$ the wave vector, and $f(E)$ is the Fermi function. The TB eigenstates $\epsilon_{n,\mathbf{k}}$ are implicitly dependent on the atomic positions through a Koster-Slater[11] expansion of the hopping elements in the TB Hamiltonian matrix $H_{ij}^{\alpha\beta}$ (where $\alpha,\beta$ label the atomic orbital symmetry and $i,j$ the atomic sites). In fact the latter can be written in terms of the direction cosines $(l,m,n)$ of the in-

 

teratomic vector $\mathbf{r}_{ij}$ and two-center integrals $V_{ij}^{\alpha\beta p}$ (diatomic molecular line) with $p$ axial symmetry ($p=\sigma,\pi,\delta$)

$$H_{ij}^{\alpha\beta}=\sum_{p} W_{ij}^{p}(lmn)V_{ij}^{\alpha\beta p}(r_{ij}). \tag{3}$$

For the radial dependence of $V_{ij}^{\alpha\beta p}$ we used the Harrison prescription[12]

$$V_{ij}^{\alpha\beta p}=V_{ij}^{\alpha\beta p}(r_{ij}^{0})\left[\frac{r_{ij}^{0}}{r_{ij}}\right]^{q_{\alpha\beta}}, \tag{4}$$

where $r_{ij}^{0}$ is the interatomic equilibrium distance with $q_{\alpha\beta}=2$ for $\alpha,\beta=s,p$; $q_{\alpha\beta}=3.5$ for $\alpha=s,p,\beta=d$ and $q_{\alpha\beta}=5$ for $\alpha,\beta=d$. These *power law* scalings are suitable in the case of small atomic displacements from the equilibrium structure (as in our case), and particularly if the hopping elements $H_{ij}^{\alpha\beta}$ are restricted to small shells of neighbors (which are mostly responsible for the equilibrium structure and lattice parameter).

$E_{\rm rep}\{\mathbf{R}\}$ represents the effective interactions generated by the incomplete cancellation of core-core and electron-electron many body terms,

$$E_{\rm rep}=E_{c\text{-}c}-E_{e\text{-}e}. \tag{5}$$

In the case of nonpolar compounds, it is short ranged and can be approximated by a sum of two-body potentials $\phi_{ij}(r_{ij})$

$$E_{\rm rep}=\sum_{i>j}\phi_{ij}(r_{ij}). \tag{6}$$

In this application we use an exponential form of $\phi_{ij}(r_{ij})$

$$\phi_{ij}(r_{ij})=\phi_{ij}\exp\left[-\alpha_{ij}\frac{|r_{ij}|}{d_0}\right], \tag{7}$$

which includes Si-metal (first neighbor) and Si-Si (second neighbor) pairs with different $\phi_{ij}$ and $\alpha_{ij}$ even if they display quite close interatomic distances in the fluorite structure ($d_0$ is the first neighbor distance).

Actually, our expression for $E_{\rm bs}$ does not take into account the modifications of the on-site terms $H_{ii}^{\alpha\alpha}$ occurring with the lattice deformation. They are mainly produced by (i) changes in the orthogonalized basis set with orbital overlap, as due to changes in atomic configuration; and (ii) charge transfer effects with atomic displacement, generating rigid shifts in the onsite elements, due to intra-atomic Hartree repulsion and interatomic crystal field potential.

A commonly accepted approximation[13] is to include these effects into the repulsive contribution $E_{\rm rep}$, which consequently requires a suitable fitting of $\phi_{ij}$ and $\alpha_{ij}$ depending on the application (small deformations, as in our case, or coordination changes, as it is in the case of cohesion energies, for example). This is the reason why we perform here an *ad hoc* adjustment of the repulsive parameters for both $CoSi_2$ and $FeSi_2$ on the available elastic and vibrational information, as reported in the next section.

The force constant matrix $\Phi_{x,x'}(i,j)$ is obtained as the second derivative of the total energy with respect to the Cartesian components $(x,x')$ of the atomic displacements $\mathbf{u}^i$ and $\mathbf{u}^j$

$$\Phi_{x,x'}(i,j)=\frac{\partial^2 E\{\mathbf{R_0}+\mathbf{u}\}}{\partial u_x^i\partial u_{x'}^j}\Big|_{\mathbf{u}=0}=\frac{\partial^2\Delta E_{\rm bs}(\mathbf{u}^i,\mathbf{u}^j)}{\partial u_x^i\partial u_{x'}^j}\Big|_{\mathbf{u}^i,\mathbf{u}^j=0}+\frac{\partial^2\Delta E_{\rm rep}(\mathbf{u}^i,\mathbf{u}^j)}{\partial u_x^i\partial u_{x'}^j}\Big|_{\mathbf{u}^i,\mathbf{u}^j=0}, \tag{8}$$

where

$$\Delta E_{\rm bs}(\mathbf{u}^i,\mathbf{u}^j)=E_{\rm bs}(\mathbf{r}_0^i+\mathbf{u}^i,\mathbf{r}_0^j+\mathbf{u}^j)-E_{\rm bs}(\mathbf{r}_0^i,\mathbf{r}_0^j),$$

$$\Delta E_{\rm rep}(\mathbf{u}^i,\mathbf{u}^j)=E_{\rm rep}(\mathbf{r}_0^i+\mathbf{u}^i,\mathbf{r}_0^j+\mathbf{u}^j)-E_{\rm rep}(\mathbf{r}_0^i,\mathbf{r}_0^j).$$

$\{\mathbf{R}_0\}$ represents the set of the equilibrium lattice sites and $\mathbf{r}_0^i$ its $i$th element. The second term in the right-hand side of Eq. (8) can be obtained after a trivial analytic derivation once the two body function describing the interatomic repulsive potentials is known. The first term, on the contrary, has to be calculated numerically, in the framework of a Green function perturbation approach, as reported in Ref. 8

$$\Delta E_{\rm bs}=\int_{-\infty}^{E_F}E[N(E)-N_0(E)]dE=\int_{-\infty}^{E_F}E\left\{-\frac{1}{\pi}\,\mathrm{Im\ Tr}[G(E)-G_0(E)]\right\}dE, \tag{9}$$

where $N(E)$ and $G(E)$ are, respectively, the electronic density of states and the Green function of the system as perturbed by two atomic displacements and $N_0(E)$ and $G_0(E)$ the corresponding unperturbed quantities. Here we disregard the variation of $E_F$ with $(\mathbf{u}^i,\mathbf{u}^j)$, since it provides a contribution to any force constant in the system which is an infinitesimal, due to the nonlocal nature of $E_F$. The second derivative of (9) gives the contribution to the force constant matrix generated by the band structure (attractive) term[8]

$$\Phi_{x,x'}^{\rm bs}(i,j)=-\frac{2}{\pi}\sum_{\alpha,\beta}\mathrm{Im}\int_{-\infty}^{E_F}\langle i\alpha|G_0(E)|j\beta\rangle\left(\frac{\partial^2}{\partial u_x^i\partial u_{x'}^j}\langle j\beta|H|i\alpha\rangle\right)dE-\frac{2}{\pi}\sum_{\alpha,\beta,\gamma,\delta}\sum_{l\neq i,m\neq j}\mathrm{Im}\int_{-\infty}^{E_F}\Bigg[\langle j\beta|G_0(E)|i\alpha\rangle$$
$$\times\left(\frac{\partial}{\partial u_x^i}\langle i\alpha|H|l\gamma\rangle\right)\langle l\gamma|G_0(E)|m\delta\rangle\left(\frac{\partial}{\partial u_{x'}^j}\langle m\delta|H|j\beta\rangle\right)+\langle i\alpha|G_0(E)|m\delta\rangle\left(\frac{\partial}{\partial u_{x'}^j}\langle m\delta|H|j\beta\rangle\right)\langle j\beta|G_0(E)|l\gamma\rangle$$
$$\times\left(\frac{\partial}{\partial u_x^i}\langle l\gamma|H|i\alpha\rangle\right)\Bigg]dE. \tag{10}$$

TABLE I. TB parameters (eV) for $FeSi_2$ in the $CaF_2$ structure.

| | $d$ (Å) | $ss\sigma$ | $sp\sigma$ | $pp\sigma$ | $pp\pi$ | $sd\sigma$ | $pd\sigma$ | $pd\pi$ | $dd\sigma$ | $dd\pi$ | $dd\delta$ |
|---|---|---|---|---|---|---|---|---|---|---|---|
| Fe-Si | 2.332 | −1.087 | 1.598 | 3.493 | −0.458 | | | | | | |
| Si-Fe | 2.332 | −1.087 | 1.660 | 3.493 | −0.458 | −1.579 | −1.302 | 0.622 | | | |
| Si-Si | 2.693 | −0.895 | 1.209 | 1.848 | −0.539 | | | | | | |
| Fe-Fe | 3.808 | −0.142 | 0.267 | 0.755 | −0.053 | −0.088 | −0.207 | 0.086 | −0.121 | 0.049 | −0.011 |
| | | $E(s)$ | $E(p)$ | $E(d)$ | | | | | | | |
| Fe | | 4.730 | 6.029 | −1.582 | | | | | | | |
| Si | | −3.925 | 4.044 | | | | | | | | |

It is easy to see that, due to the limited range of TB interactions, the first term in (10), which we call $\Phi^{bs}_{SR}$, describes the short range action of the covalent bonding whereas the second term, which we call $\Phi^{bs}_{LR}$, provides the long range effects of the electronic susceptibility. The range of $\Phi^{bs}_{LR}$ critically depends on the DOS at the Fermi level and it is larger in metallic silicides than in semiconductors like silicon.[8] A check of convergence is provided by the translational invariance condition applied to $\Phi^{bs}_{LR}$

$$\Phi^{bs}_{LR}(i,i) = -\sum_{j\neq i} \Phi^{bs}_{LR}(i,j), \tag{11}$$

which relates the diagonal element, straightforwardly evaluated through Eq. (10), to all the others. The degree of approximation in fulfilling Eq. (11) sets the force constant range.

By taking advantage of crystal periodicity we calculate $G_0(E)$ from its spectral formula in $\mathbf{k}$ vector space

$$G_0(E) = \lim_{\epsilon\to 0^+} \sum_{n,\mathbf{k}} \frac{|n\mathbf{k}\rangle\langle n\mathbf{k}|}{E-\epsilon_{n,\mathbf{k}}+i\epsilon}, \tag{12}$$

where $|n\mathbf{k}\rangle$ are the electronic Hamiltonian eigenvectors, and we also perform the Fourier transforms of $\Phi^{bs}_{LR}, \Phi^{bs}_{SR}, \Phi^{rep}$. From their sum the phonon dispersion relations in the irreducible part of the Brillouin zone are finally obtained.

### III. APPLICATION TO $CoSi_2$ AND $FeSi_2$

In the fluorite structure, the metal atoms ($M$) are tetrahedrally coordinated around the Si sites and $M$ is inside a cubic cage of first neighbor silicon atoms. The bulk lattice parameter $a_0$ of the ideal $FeSi_2$ is obtained by *ab initio* prediction[14] as $a_0 = 5.387$ Å and 5.364 Å is the experimental value[15] for $CoSi_2$. The interatomic distances are $d_{M\text{-Si}} = \sqrt{3}/4 a_0$, $d_{\text{Si-Si}} = 1/2 a_0$ and $d_{M\text{-}M} = 1/\sqrt{2} a_0$, so that the first-neighbor ($M$-Si) and second-neighbor (Si-Si) distances are not very different, but $d_{M\text{-}M}$ is considerably larger. Therefore the repulsive potential is limited to $M$-Si and Si-Si pairs, whereas the TB hoppings include also $M$-$M$ interactions, which are important for a correct description of the density of states at the Fermi level. As in our previous works[16,17] we use indeed an extended basis set ($sp^3$ for Si and $sp^3d^5$ for the metal atom), but here we also include $d$-$d$ hopping elements between metallic pairs, besides $pp\sigma$ long range interactions. In this way a better fit of the *ab initio* band structure calculations for (CsCl)FeSi, fluorite $FeSi_2$ (Refs. 6,14) and fluorite $CoSi_2$ is obtained,[2] and very satisfactory predictions of total energy calculations for different crystal phases of iron and cobalt silicides have been produced.[5,18] In Table I we give the tight-binding parameters employed in our calculation for $FeSi_2$ and in Table II we give those for $CoSi_2$.

The electronic information which enters our method can be well represented by the electronic DOS, as estimated by the imaginary part of the Green function calculated over a mesh of 1300 $\mathbf{k}$ points in the irreducible part of the Brillouin zone. In Fig. 1 we present the DOS for $CoSi_2$ (top) and $FeSi_2$ (bottom). One notes the similarity between the spectra of the two crystals, but for the Fermi energy falling in a region of higher density in the case of $FeSi_2$.

As mentioned in the previous section, the repulsive potential adopted here is different in form and parameters with respect to the one we used in Refs. 5 and 18. In that case we required $\phi_{ij}(\mathbf{r}_{ij})$ to fulfill the equilibrium and stability conditions with respect to isotropic deformations in different crystal structures. This is a good procedure in order to obtain

TABLE II. TB parameters (eV) for $CoSi_2$ in the $CaF_2$ structure.

| | $d$ (Å) | $ss\sigma$ | $sp\sigma$ | $pp\sigma$ | $pp\pi$ | $sd\sigma$ | $pd\sigma$ | $pd\pi$ | $dd\sigma$ | $dd\pi$ | $dd\delta$ |
|---|---|---|---|---|---|---|---|---|---|---|---|
| Co-Si | 2.323 | −1.140 | 1.460 | 2.940 | −0.800 | | | | | | |
| Si-Co | 2.323 | −1.140 | 2.090 | 2.940 | −0.800 | −1.210 | −1.180 | 0.700 | | | |
| Si-Si | 2.682 | −0.975 | 1.140 | 1.540 | −0.580 | | | | | | |
| Co-Co | 3.794 | −0.136 | 0.270 | 0.783 | −0.054 | −0.084 | −0.205 | 0.087 | −0.081 | 0.046 | 0.012 |
| | | $E(s)$ | $E(p)$ | $E(d)$ | | | | | | | |
| Co | | 2.986 | 8.476 | −2.254 | | | | | | | |
| Si | | −4.924 | 1.856 | | | | | | | | |

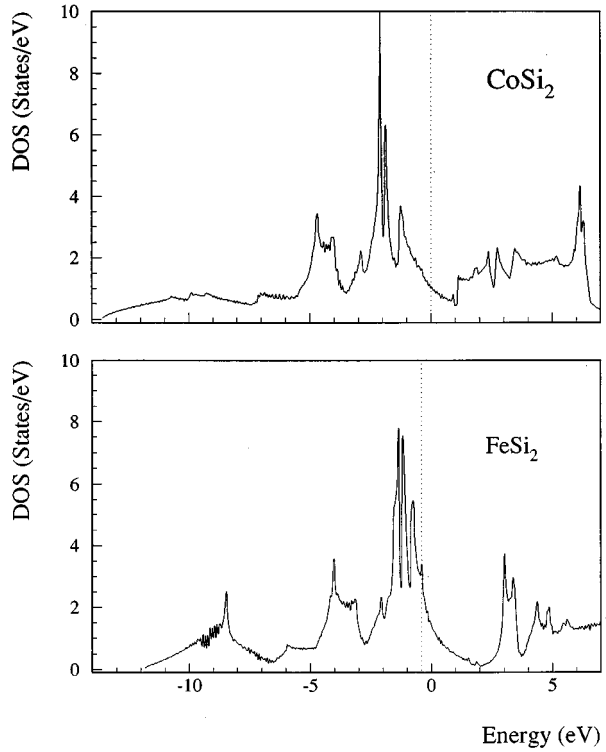


FIG. 1. Tight-binding density of states for $CoSi_2$ (top) and $FeSi_2$ (bottom). The vertical dotted line indicates the position of the Fermi level.

a highly transferable potential, still it gives quite a poor reproduction of the shear deformations and the vibrational frequencies of one particular phase [especially if $\phi_{ij}(\mathbf{r}_{ij})$ is a purely central force constant, as in our case]. Therefore we include here the elastic and optical data in the fitting procedure, whenever they are experimentally available, as it is the case of $CoSi_2$.

Since the parameters $\phi$ and $\alpha$ of Eq. (7) are different for Si-*M* and Si-Si interactions, we need at least four fitting data: two of them are provided by the equilibrium and stability relations, involving the first and second derivatives of the total energy, with the equilibrium lattice parameter and the bulk modulus.[6] The remaining two parameters are fitted by means of a multivalued $\chi^2$ minimization to the elastic constants $c_{44}$, $c_{11}$-$c_{12}$, and to the Raman and infrared phonon frequencies at the $\Gamma$ point. Actually, we perform the fitting in $CoSi_2$ by assigning different weights to the reference data as we have contrasting experimental estimations for $B$, $c_{44}$, and $c_{11}$-$c_{12}$,[19,20] whereas the optical data[21] are very accurate and recently confirmed by *ab initio* frozen phonon calculations.[22]

TABLE III. Lattice constants and repulsive parameters $\phi$ an $\alpha$ for $CoSi_2$ and $FeSi_2$.

| | $a_0$Å | | $\phi$ (eV) | $\alpha$ |
|---|---|---|---|---|
| $CoSi_2$ | 5.365 | Co-Si | 4590 | 8.05 |
| | | Si-Si | 165 | 4.12 |
| $FeSi_2$ | 5.387 | Fe-Si | 6150 | 8.23 |
| | | Si-Si | 635 | 5.47 |

TABLE IV. Calculated elastic constants and bulk modulus, as compared to the existing experimental and theoretical data. The values are expressed in Mbar.

| | | $B$ | $c_{11}$ | $c_{12}$ | $c_{44}$ |
|---|---|---|---|---|---|
| $CoSi_2$ | Expt. (Ref. 20) | 1.69 | 2.28 | 1.40 | 0.83 |
| | This work | 1.70 | 2.10 | 1.50 | 0.60 |
| $FeSi_2$ | Theor. (Ref. 16) | 2.06 | 2.64 | 1.77 | 0.78 |
| | This work | 1.98 | 2.80 | 1.57 | 0.67 |

In the case of $FeSi_2$ no optical nor elastic information is available, since the films are too thin ($<20$ Å) and large strain fields may also affect any possible measurement. Therefore we have to rely on the theoretical information for the ideal bulk structure. First principles calculations[6,14] provide an affordable estimation of $a_0$ and $B$ but no elastic constants. However, previous calculations for $NiSi_2$, $CoSi_2$, and $FeSi_2$ within a tight-binding scheme with a reduced set of attractive and repulsive parameters[16] gave a very satisfactory semiempirical estimation of $c_{11}$, $c_{12}$, and $c_{44}$ for $NiSi_2$ and $CoSi_2$. So we take these predictions for $c_{11}$, $c_{12}$, and $c_{44}$ of fluorite $FeSi_2$ as input values for the fitting procedure, with the additional requirement that the vibrational modes at $\Gamma$ are not higher in frequency than the corresponding modes in stable, more compact, $\beta$ phase. We are aware that this estimation of the repulsive parameters seems barely qualitative, still we will see in the following that the real difference between $CoSi_2$ and $FeSi_2$ rests on the long range contribution of the band structure term. Moreover, the large similarity in the repulsive parameters obtained for both materials is not surprising on the basis of the physical argument that they describe nearly atomic properties at short range, which should not be affected by the different position

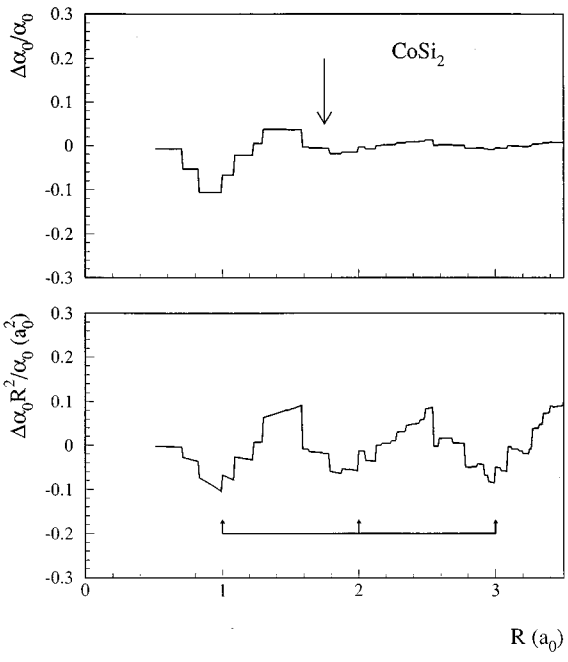


FIG. 2. Variation of the diagonal force constant on the metallic site with respect to the increasing cutoff radius for $CoSi_2$ (see text).

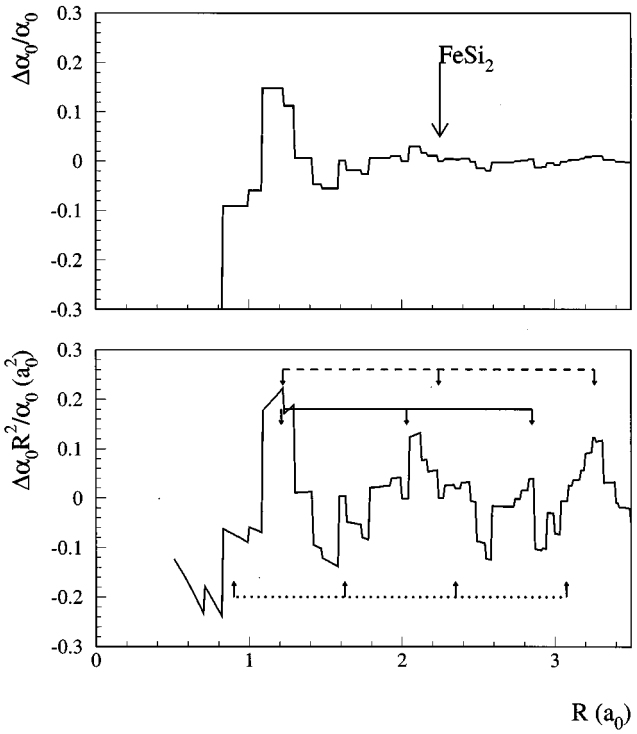


FIG. 3. Variation of the diagonal force constant on the metallic site with respect to the increasing cutoff radius for $FeSi_2$ (see text).

of the Fermi level in the two materials. In Tables III and IV we report, respectively, the repulsive parameters and the reproduction of the input elastic constants obtained by our fitting. They have been calculated for a suitable cutoff radius in the long range part of the attractive term, as will be discussed in the next session.

## IV. THE LONG RANGE INTERACTION

In Figs. 2 and 3 (top panels) we report the difference between the left and right side of Eq. (11) for a diagonal force constant of the metallic site, in $CoSi_2$ and $FeSi_2$ respectively, as a function of the increasing range in the off diagonal elements. It is expressed as the percentage variation with respect to the total $\Phi_{xx}(i,i)$, which includes $\Phi^{bs}_{LR}(i,j)$,$\Phi^{bs}_{SR}(i,j)$ and $\Phi^{rep}(i,j)$, and indicates the convergence behavior of $\Phi^{bs}_{LR}(i,j)$ at large distances, where it represents the only contribution to the total force constant matrix. We note that, at variance to the case of semiconductors like silicon,[8] a slow convergence with sizeable oscillations is obtained, especially in the case of $FeSi_2$. These oscillations, however, are not random fluctuations due to numerical errors, but represent the Friedel oscillations in the charge density of the system, originated by the perturbation induced by the atomic displacement. In Figs. 2 and 3 (bottom panels) we show the same quantity weighted by the square of the increasing interatomic distance, in order to amplify the long range oscillations and to simulate their effect on the elastic constants ( and bulk modulus $B$). We see that in the case of $CoSi_2$ one periodicity is present (indicated by the small arrows), whereas in $FeSi_2$ at least two of them are superimposed, probably even more. Actually the progressive summa-

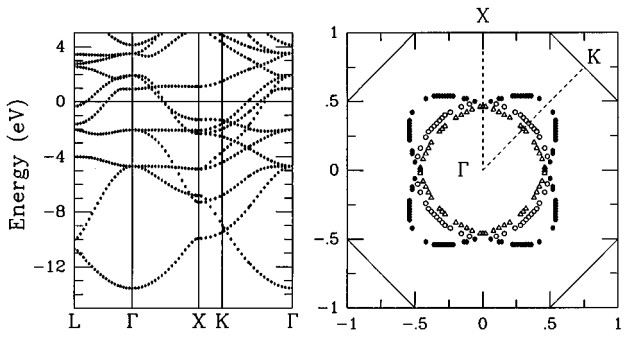


FIG. 4. Tight-binding electronic bands (left) and (001) cut of the Fermi surface for the three topmost occupied bands (right) in $CoSi_2$.

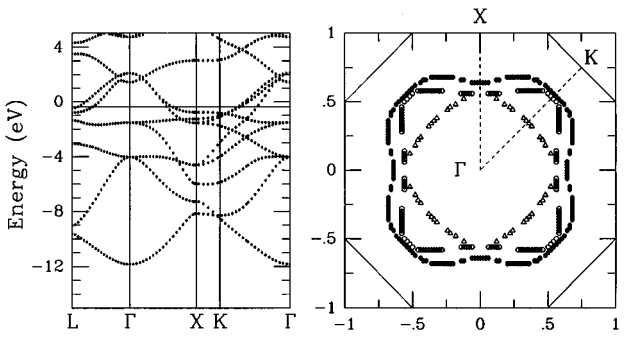


FIG. 5. Tight-binding electronic bands (left) and (001) cut of the Fermi surface for the three topmost occupied bands (right) in $FeSi_2$.

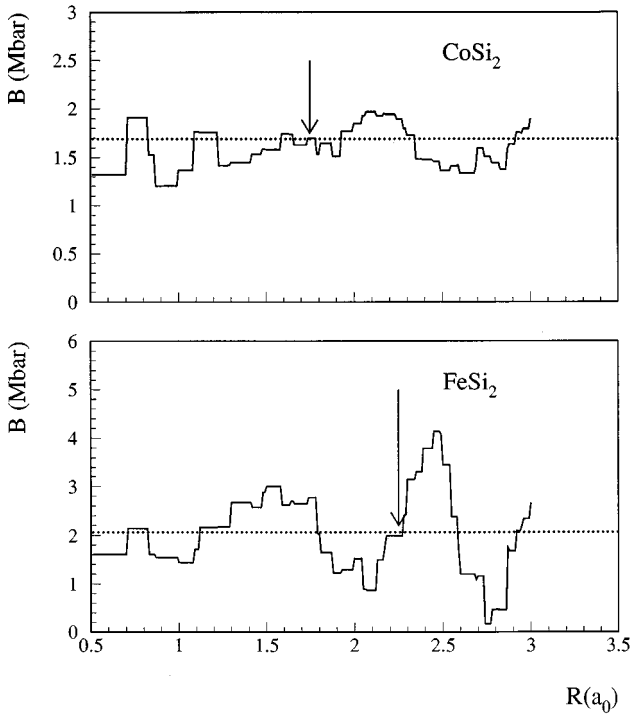


FIG. 6. Cutoff radius dependence of the calculated bulk modulus for $CoSi_2$ (upper panel) and $FeSi_2$ (lower panel).

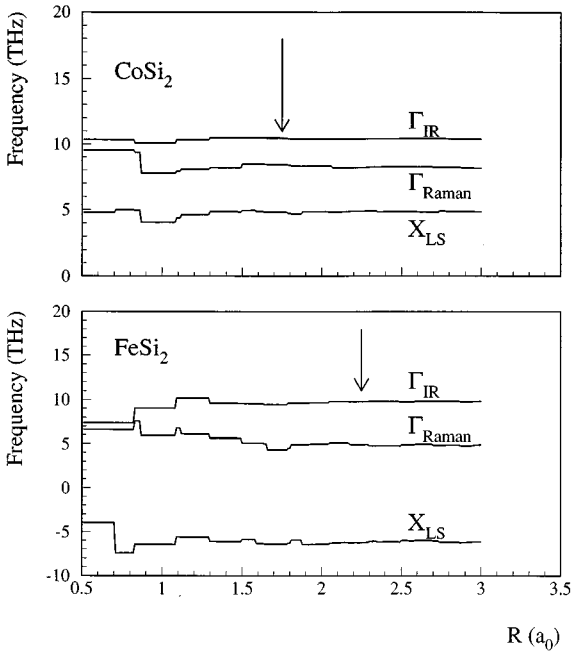


FIG. 7. Cutoff radius dependence of the calculated infrared and Raman modes at $\Gamma$ and of the lowest mode at the $X$ point for $CoSi_2$ (upper panel) and $FeSi_2$ (lower panel).

tion of the interatomic force constants for spherical shells with increasing radius allows a rough estimate of the oscillating behavior in the second derivative of the interatomic potential, as produced by the enhanced electronic susceptibility for virtual electronic transitions within the Fermi surface. The presence of large flat portions of the Fermi surface with nesting vectors of $2k_F$ is in turn necessary for such an effect. This occurs in $CoSi_2$ and $FeSi_2$ as reported in the right panels of Figs. 4 and 5, respectively, where we show a (001) cut of the Fermi surface for the three top occupied

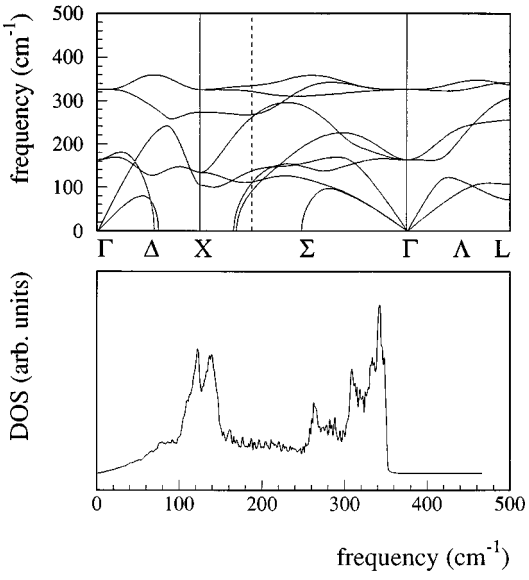


FIG. 9. Phonon dispersion relations (upper panel) and density of states (lower panel) in $FeSi_2$.

bands (left panels). We note that in $CoSi_2$ only one nesting vector for the topmost (square) band is relevant and corresponds exactly to the periodicity in Fig. 2 ($k^{osc}=1.0\times 2\pi a_0^{-1}$). On the contrary three nesting vectors are evident for the three topmost bands in $FeSi_2$, in qualitative agreement to Fig. 3 ($k_1^{osc}=1.38\times 2\pi a_0^{-1}$, $k_2^{osc}=1.23\times 2\pi a_0^{-1}$, and $k_3^{osc}=1.04\times 2\pi a_0^{-1}$).

In a real space picture these charge oscillations are produced by any structural defect within the system, and, in turn, they provide some distortive force to the lattice. From this point of view it is interesting to note that the oscillations in Figs. 2 and 3 are, respectively, commensurate and incommensurate with respect to the fluorite lattice, with a rough phase shift by $\pi$ extending down to the first and second

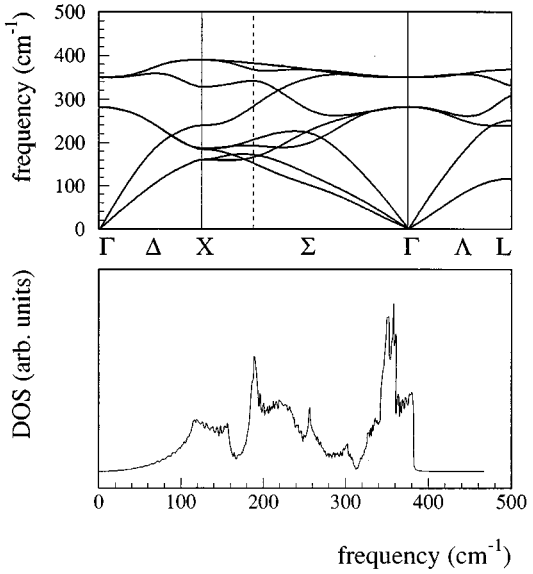


FIG. 8. Phonon dispersion relations (upper panel) and density of states (lower panel) in $CoSi_2$.

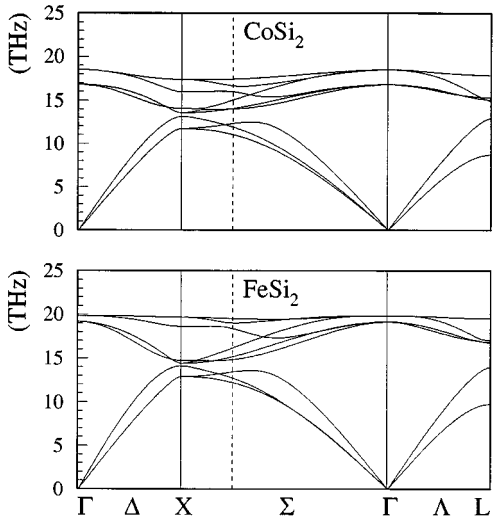


FIG. 10. Effect of the exclusion of $\Phi_{LR}^{bs}$ from the total force constant matrix on the dispersion curve of fluorite $CoSi_2$ (top) and $FeSi_2$ (bottom).

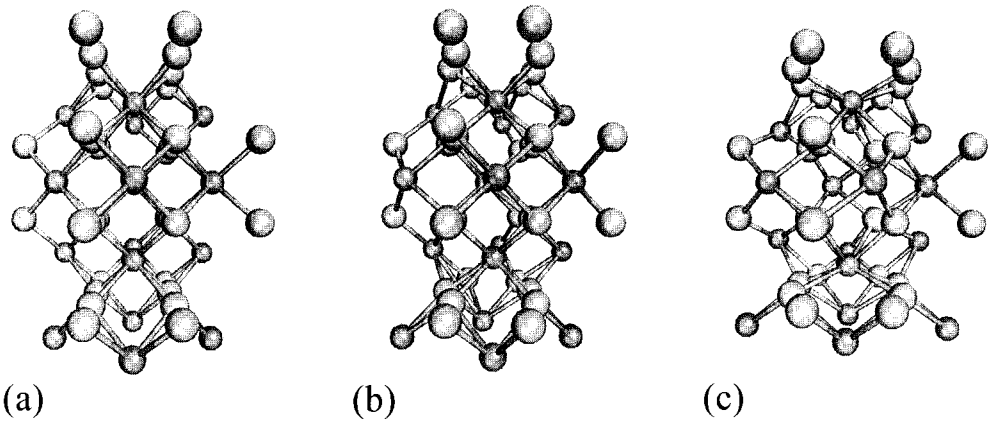


FIG. 11. Lattice configuration of fluorite (a), $\beta$-$FeSi_2$ (c), and LO soft mode configuration at $\mathbf{k}\approx(0.5,0.5,0)$ (b). Si atoms are represented by big, bright spheres.

neighbor shells (not shown here). We conclude that this charge distribution, whatever originated in the real system, plays a destabilizing action only in $FeSi_2$, where larger flat portions of the Fermi surface and a higher density of states at the Fermi level even enhance this effect.

## V. RESULTS

In Fig. 6 we display the behavior of $B$ as a function of the cutoff radius for $CoSi_2$ (top panel) and $FeSi_2$ (bottom panel). It is calculated as function of the elastic constants which, in turn, are obtained through the Born expansion at long wavelengths in terms of the force constants.[23] Therefore it is reasonable to find the same large oscillations as in the bottom panels of Figs. 2 and 3. When we selected the cutoff radius for the fitting procedure of the repulsive potential we had to balance the computational load with the convergent behavior in the long range force constant. Our choice for $CoSi_2$ and $FeSi_2$ is indicated by arrows in the top panels of Figs. 2 and 3 and in Fig. 6, where the dotted line indicates the fitting value of $B$. We are aware that true convergence cannot be achieved in the elastic constants, still the phonon dispersion relations do not change appreciably, both in $CoSi_2$ and $FeSi_2$, for larger values of the cutoff radius with respect to the one we selected. In Fig. 7 we report the behavior of the infrared and Raman modes in $\Gamma$ as a function of the cutoff radius and we see that a converged value is obtained within our choice (indicated by the vertical arrow). This is true even for vibrations outside the $\Gamma$ point and the behavior of the lowest mode at the $X$ point, $X_{\mathrm{LS}}$ in Fig. 7, confirms our statement. For what concerns the latter, we see that in the case of $FeSi_2$ (lower panel) the frequency converges to an imaginary value (negative axis in our figure), pointing out that the fluorite structure displays phonon instabilities.

This fact is clearly reported in Figs. 8 and 9 where phonon dispersion relations (top panel) and the phonon DOS (bottom panel) for $CoSi_2$ and $FeSi_2$, respectively, are displayed. In the latter case we note that the $LO_1$ and $TO_1$ branches, giving rise to the Raman mode at $\Gamma$, are dramatically softened to imaginary frequencies along $\Delta$ and $\Sigma$ directions, where a relevant hybridization with the TA phonons is also present. We can straightforwardly address the source of this phonon instability in $FeSi_2$ with respect to $CoSi_2$ to $\Phi^{\mathrm{bs}}_{\mathrm{LR}}$. In fact, if we compare the phonon dispersion relations originated by $\Phi^{\mathrm{bs}}_{\mathrm{SR}}+\Phi^{\mathrm{rep}}$ both in $CoSi_2$ and $FeSi_2$ (top and bottom panels of Fig. 10, respectively) we note that no sizeable differences exist. Therefore it is the long range contribution, no matter how large is the cutoff radius, which destabilizes the $TO_1$ and $LO_1$ branches. In particular we analyzed all the displacement patterns of the modes with zero frequency and we found that the $LO_1$ phonon at $k\approx(1/2,1/2,0)$ along $\Sigma$ provides a displacement pattern which is qualitatively similar to the one occurring in the structural distortion from fluorite to orthorhombic $FeSi_2$. In Fig. 11 we compare a (110) view of the equilibrium fluorite structure [panel (a)], the phonon distorted fluorite structure [panel (b)] and the $\beta$ structure [panel (c)]. Several features of the latter are already present in the second one. In the case of $CoSi_2$ no imaginary frequency is present, according to the fact that it is stable in the $CaF_2$ phase. Still the dispersion of the $LO_1$ and $TO_1$ modes is very sensitive to the description of the electronic states even in this case and a previous calculation by some of the authors with a reduced set of TB parameters and a smaller cutoff radius[17] provided a different behavior only for these modes. Therefore we may conclude that the electron-phonon interaction is particularly effective for $LO_1$ and $TO_1$ modes even in $CoSi_2$. The different position of the Fermi level in $FeSi_2$ is, however, the key feature to understand the instability of the fluorite structure. In fact, this particular ratio of $d$ electrons per atom provides a high density of states at the Fermi level and a large electronic susceptibility at $2k_F$ which, in turn, give rise to charge density waves not commensurate with the lattice. In the meantime the long range part of the force constant matrix is modified to the extent that a phonon instability is generated in the system. Finally, and apparently not related to the instability of the pretransformation phase, even in the target semiconducting structure, the Fermi level is suitably positioned right in the gap, providing a Jahn-Teller energy gain which is not allowed to an ideal $\beta$-$CoSi_2$, where the Fermi level would be shifted in the conduction band.

**ACKNOWLEDGMENTS**

We are grateful to L. Colombo (Univ. of Milan) and F. Marabelli (Univ. of Pavia) for helpful discussions. This work was partially supported by the Human Capital and Mobility program of the European Community through Contract No. CHRX-CT93-0110. One of us (S.S.) thanks the Instituto de Ciencia de Materiales (Madrid, Spain) for the kind hospitality.

---

*Present address: SGS–Thomson Microelectronics, 20400 Agrate, Milano, Italy.

†Permanent address: Instituto de Ciencia de Materiales, CSIC, Cantoblanco, 28049 Madrid, Spain.

[1] H. von Kaenel, Mater. Sci. Rep. **8**, 193 (1992).

[2] W. R. Lambrecht, N. E. Christensen, and R. Blochl, Phys. Rev. B **36**, 2493 (1987).

[3] P.Y. Dusausoy, J. Protas, R. Wandji, and R. Roques, Acta Crystallogr. B **27**, 1209 (1971).

[4] H. von Kaenel, R. Stalder, H. Sirringhaus, N. Onda, and J. Henz, Appl. Surf. Sci. **53**, 196 (1991); A. L. Vazquez de Parga, J. De la Figuera, C. Ocal, and R. Miranda, Europhys. Lett. **18**, 595 (1992); Le Thanh Vinh, J. Chevrier, and J. Derrien, Phys. Rev. B **46**, 15 946 (1992); H. Ch. Schaefer, B. Roesen, H. Moritz, A. Rizzi, B. Lengeler, H. Luth, and D. Gerthsen, Appl. Phys. Lett. **62**, 2271 (1993).

[5] L. Miglio, F. Tavazza, and G. Malegori, Appl. Phys. Lett. **67**, 2293 (1995).

[6] N.E. Christensen, Phys. Rev. B **42**, 7148 (1990).

[7] L. Miglio, F. Tavazza, and M. Celino (unpublished).

[8] A. Mazur and J. Pollmann, Phys. Rev. B **39**, 5261 (1989).

[9] K.C. Hass, Phys. Rev. B **46**, 139 (1992).

[10] M.W. Finnis, K.L. Kear, and D.G. Pettifor, Phys. Rev. Lett. **52**, 291 (1984); C.M. Varma and W. Weber, Phys. Rev. B **19**, 6142 (1979).

[11] J.C. Slater and G.F. Koster, Phys. Rev. **94**, 1498 (1954).

[12] W. A. Harrison, *Electronic Structure and the Properties of Solids* (Freeman, San Francisco, 1980).

[13] M.W. Finnis, A.T. Paxton, D.G. Pettifor, A.P. Sutton, and Y. Ohta, Philos. Mag. A **58**, 143 (1988).

[14] K. A. Maeder, H. Von Kaenel, and A. Baldareschi, Phys. Rev. B **48**, 4364 (1993).

[15] *Properties of Metal Silicides*, edited by K. Maex and M. von Rossum (INSPEC, London, 1995).

[16] G. Malegori and L. Miglio, Phys. Rev. B **48**, 9223 (1993).

[17] S. Sanguinetti, C. Calegari, and L. Miglio, Appl. Surf. Sci. **91**, 103 (1995).

[18] H. von Kaenel, C. Schwarz, S. Goncalves-Couto, E. Mueller, L. Miglio, F. Tavazza, and G. Malegori, Phys. Rev. Lett. **74**, 1163 (1995).

[19] L. Weiss, A.Yu. Rumyantsev, and A.S. Ivanov, Phys. Status Solidi B **128**, K111 (1985).

[20] G. Guenin, M. Ignat, and O. Thomas, J. Appl. Phys. **68**, 6515 (1990).

[21] S. Bocelli, G. Guizzetti, F. Marabelli, G. Thungström, and C.S. Petterson, Appl. Surf. Sci. **91**, 30 (1995).

[22] V. Milman, M.H. Lee, and M.C. Payne, Phys. Rev. B **49**, 16 300 (1994).

[23] M. Born and K. Huang, *Dynamical Theory of Crystal Lattices* (Clarendon, Oxford, 1954).